Uncertainty Quantification of Thermoacoustic Instabilities in a Swirled Stabilized Combustor

A. Ndiaye, M. Bauerheim, S. Moreau, Franck Nicoud

Proceedings of ASME Turbo Expo 2015: Turbine Technical Conference and Exposition
GT2015
June 15 – 19, 2015, Montréal, Canada

UNCERTAINTY QUANTIFICATION OF THERMOACOUSTIC INSTABILITIES IN A SWIRLED STABILIZED COMBUSTOR

A. NDIAYE
CERFACS
Toulouse, Midi-Pyrénées, FRANCE
Email: ndiaye@cerfacs.fr

M. BAUERHEIM
CERFACS
Toulouse, Midi-Pyrénées, FRANCE
Email: bauerheim@cerfacs.fr
and
SNECMA
Villaroche, FRANCE
Email: michael.bauerheim@snecma.fr

S. MOREAU
University Sherbrooke
Sherbrooke, Québec, CANADA
Email: stephane.moreau@USherbrooke.ca

F. NICOUD
I3M UMR-CNRS 5149
University Montpellier II,
Montpellier, Languedoc-Roussillon, FRANCE
Email: franck.nicoud@univ-montp2.fr

ABSTRACT

Combustion instabilities can develop in modern gas-turbines as large amplitude pressure oscillations coupled with heat release fluctuations. In extreme cases, they lead to irreversible damage which can destroy the combustor. Prediction and control of all acoustic modes of the configuration at the design stage are therefore required to avoid these instabilities. This is a challenging task because of the large number of parameters involved. This situation becomes even more complex when considering uncertainties of the underlying models and input parameters. The forward uncertainty quantification problem is addressed in the case of a single swirled burner combustor. First, a Helmholtz solver is used to analyze the thermoacoustic modes of the combustion chamber. The Flame Transfer Function measured experimentally is used as a flame model for the Helmholtz solver. Then, the frequency of oscillation and the growth rate of the first thermoacoustic mode are computed in 24 different operating points. Comparisons between experimental and numerical results show good agreements except for modes which are marginally stable/unstable. The main reason is that the uncertainties can arbitrary change the nature of these modes (stable vs unstable) ; in other words, the usual mode classification stable/unstable must be replaced by a more continuous description such as the risk factor, i.e. the probability for a mode to be unstable given the uncertainties on the input parameters. To do so, a Monte Carlo analysis is performed using 4000 Helmholtz simulations of a single experimental operating point but with random perturbations on the FTF parameters. This allows the computation of the risk factor associated to this acoustic mode. Finally, the analysis of the Monte Carlo database suggests that a reduced two-step UQ strategy may be efficient to deal with thermoacoustics in such a system. First, two bilinear surrogate models are tuned from a moderate number of Helmholtz solutions (a few tens). Then, these algebraic models are used to perform a Monte Carlo analysis at reduced cost and approximate the risk factor of the mode. The accuracy and efficiency of this reduced

UQ strategy are assessed by comparing the reference risk factor given by the full Monte Carlo database and the approximate risk factor obtained by the surrogate models. It shows a good agreement which proves that reduced efficient methods can be used to predict unstable modes.

NOMENCLATURE

Abbreviations

UQ Uncertainty Quantification
FTF Flame Transfer Function
RF Risk Factor
LES Large Eddy Simulation
PDF Probability Density Function
S Stable regime
U Unstable regime
S/U Marginally stable regime

Symbols

f_0 Initial complex frequency
p_1 Complex pressure amplitude
q_1 Heat release fluctuations
$\hat{p}$ Harmonic complex pressure amplitude
$\hat{q}$ Harmonic heat release fluctuations
p_0 Mean pressure
c_0 Mean field of sound speed
n FTF amplitude
$\bar{n}$ Mean FTF amplitude
f^U Probability density function of the continuous uniform distribution
f^β Probability density function of the β-distribution
B The beta function
Γ The gamma function
R_U Range of the uniform distribution
R_B Range of the β-distribution
$\Re$ Real part
$\Im$ Imaginary part
Corr Correlation coefficient

Subscripts

X Random variable
Y Random variable
$\tilde{Y}$ The mean of Y
t Transpose operator

Greek letters

ρ_0 Mean density
ω Complex angular frequency
ω_0 Complex angular frequency without flame coupling
ω_r Real part of ω : Pulsation of acoustic pressure wave
ω_i Imaginary part of ω : Growth rate of the acoustic pressure disturbances
τ FTF time delay
$\bar{\tau}$ Mean FTF time delay
γ Specific heat ratio
α Shape parameter of the β-distribution
β Shape parameter of the β-distribution
α_A Acoustic losses rate of the flame A
α_B Acoustic losses rate of the flame B
Δ_α Uncertainty of the acoustic losses rate
μ^U Mean value of the uniform distribution
ν^U Variance of the uniform distribution
μ^β Mean value of the β-distribution
ν^β Variance of the β-distribution

1 INTRODUCTION

Combustion instabilities remain an active research domain for industries that involve combustion processes. They refer to the sustained acoustic fluctuations in combustors where unsteady combustion takes place. Usually this problem arises once the full combustor is tested, thus requiring expensive modifications on either the fuel injection system or the combustion chamber itself. Therefore, combustion instabilities have to be tackled at the design stage. However, this problem remains difficult because of the non-linearities associated with the turbulent flow or chemical reactions, the complex interactions between acoustics and unsteady heat-release, impedance boundary conditions as well as the numerous parameters involved. This issue becomes even more challenging when considering uncertainties on input parameters and underlying models. Especially, flame models obtained experimentally or numerically are known to be uncertain. Addressing the sensitivity of thermoacoustic results with respect to the input parameters is thus a necessary and important step towards reliable predictions of unstable modes in gas turbines. This is illustrated in Fig. 1 showing a typical result of a thermoacoustic analysis, i.e. a set of modes, each with its own frequency and growth rate. When no uncertainty is present, each

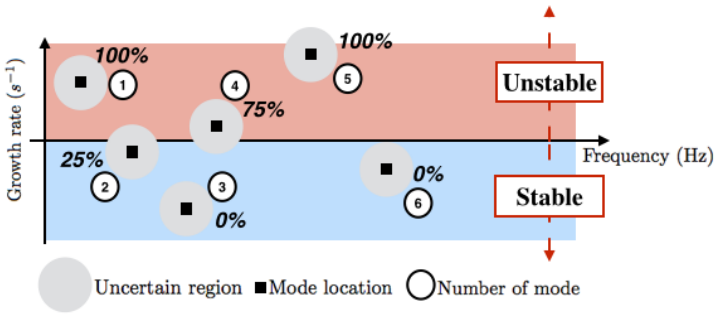

FIGURE 1. Location of the first six thermo-acoustic modes in a typical combustor.

mode corresponds to a single point (black symbols) in the frequency plane. Here, modes 1, 4 and 5 are dangerous and should be also controlled since the growth rate ω_i is positive. If uncertainties are present, each mode belongs to an admissible region of the frequency plane. Mode 2 (and maybe 6) are now dangerous and should be controlled. It suggests that taking into account uncertainties is required for reliable predictions of combustion instabilities. The objectives of this paper is therefore to (1) determine the uncertain region of the acoustic modes of a single swirled burner combustor using a brute force approach and (2) propose a methodology to deal with uncertainties at lower cost. This paper is organized as follows : the thermoacoustic framework used in this study is described in section 2 and section 3 presents the single swirled combustor configuration. The fourth section deals with the brute force Monte Carlo methodology applied to evaluate the uncertain region associated to the acoustic mode of interest. A statistical convergence study shows that 4000 Helmholtz simulations are required. It suggests that such a method can become CPU-demanding for more complex configurations using multiple uncertain parameters. In section 5, two surrogate models are tested to avoid expensive brute force methods. The purpose is to compute uncertain region of the acoustic mode with an affordable number of simulations. Finally, the prediction and the accuracy of the low-order models are validated against the initial full Monte Carlo analysis in the section5.

2 Thermoacoustic framework

Thermoacoustic instabilities can be studied using several approaches : theoretical models, low-order network methods, full scale Large Eddy Simulations, or experiments. Analytical approaches [**?**] allow the study of the underlying processes leading to combustion instabilities. However, numerous assumptions (null Mach Number, linear framework etc.) are required to simplify the problem and hence only academic or simplified configurations can be investigated. These assumptions can be relaxed using Large Eddy Simulation to predict turbulent flames interacting with the acoustic waves and reproduce self-excited combustion instabilities. However, even when LES simulations confirm that a combustor is unstable, they do not suggest how to control the instability. Moreover, LES techniques are CPU demanding : for example, performing parametric studies using hundreds of simulations is out of reach today. Faster tools such as acoustic solvers [?] are thus required to simplify the design process of the system. To do so, a linear wave equation for small pressure perturbations $p_1(x,t)$ can be derived from the reactive Navier-Stokes equations by neglecting turbulence and viscous effects and assuming a frozen baseline flow [?] :

$$\nabla.\left(\frac{1}{\rho_0}\nabla p_1\right) - \frac{1}{\gamma p_0}\frac{\partial^2 p_1}{\partial t^2} = -\frac{\gamma-1}{\gamma p_0}\frac{\partial q_1}{\partial t} \tag{1}$$

where q_1 is the heat release fluctuation. Assuming harmonic pressure ($p_1 = \hat{p}(\mathbf{x})e^{i\omega t}$) and heat release fluctuations ($q_1 = \hat{q}(\mathbf{x})e^{i\omega t}$), Eq. (1) becomes :

$$\nabla.\left(\frac{1}{\rho_0}\nabla \hat{p}\right) + \frac{\omega^2}{\gamma p_0}\hat{p} = i\omega\frac{\gamma-1}{\gamma p_0}\hat{q}(\mathbf{x}) \tag{2}$$

where $\hat{p}$ and $\hat{q}$ are the complex amplitude of the pressure and heat release disturbance and $\omega = 2\pi f$ is the complex angular frequency of the thermoacoustic mode. The density ρ_0 and the specific heat ratio γ can depend on space $\mathbf{x}$ and are known quantities related to the baseline flow ; the thermodynamic pressure p_0 is constant under the zero Mach number assumption. In Eq. (2), the right hand side term is closed by a Flame Transfer Function using the n-τ model [?].
The expression of the global FTF reads :

$$\mathscr{F}(\omega) = n(\omega)e^{i\omega\tau(\omega)} \tag{3}$$

where n is the amplitude of the flame response and τ corresponds to a time delay. These parameters n and τ are usually obtained from experiment or LES simulations. They are known to control combustion instabilities although being uncertain. One objective of this paper is to assess the sensitivity of the computed complex angular frequency to these uncertain parameters. To do so, a Helmholtz solver called AVSP [**?**] is used to solve the wave equation (Eq. (2)) in a 3D single swirled burner geometry. The outputs of the solver are the pressure field $\hat{p}$ and the complex angular frequency ω of the acoustic mode : its real part ω_r corresponds to the frequency of oscillation and ω_i is the growth rate of the acoustic disturbances. AVSP is used to study how the uncertainties on n and τ propagate into uncertainties on the growth rate ω_i and to determine the risk factor of the acoustic mode i.e. the probability for a mode to be unstable ($\omega_i > 0$) :

$$\text{risk factor}(\%) = 100\int_0^\infty PDF(\omega_i)d\omega_i \tag{4}$$

Where $PDF(\omega_i)$ stands for the Probability density function of the growth rate of the acoustic disturbances. To fairly assess the risk factor, it is necessary to have a realistic statistical distribution of the input parameters n and τ, given here by the experiment presented in the following section.

3 The single swirled burner configuration

The experimental configuration targeted in this paper corresponds to a single injector combustor designed and studied by Palies et al. [**?**] (Fig. 2). It comprises a confined swirled flame,

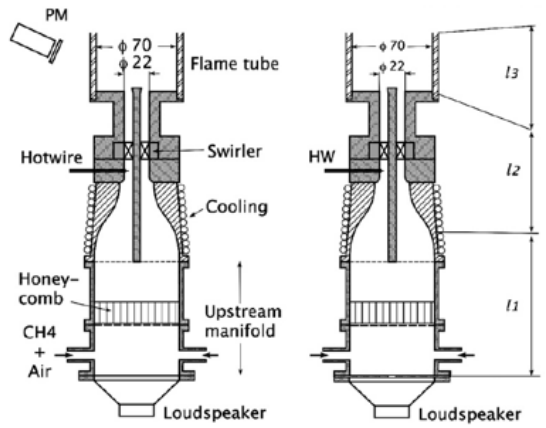

FIGURE 2. Numerical/experimental configuration. From ref. [**?**]

an upstream manifold, an injection unit equipped with a swirler and a cylindrical flame tube. The geometry of the combustor is displayed in Fig. 2. In order to ease the numerical study, the system was decomposed in three dimensional coupled tubes with variable lengths. The length l_2 which corresponds to the axisymmetric convergent tube is fixed. The length l_1 corresponds to the upstream manifold which is designed to have three different lengths and the combustion chamber l_3 may have four different lengths. This leads to twelve different set-ups, presented in Table. 1. Additionally, two different air flow rates were experimentally tested leading to flame A and B, the former with a smaller power than the latter. Finally, 24 operating points were studied for this configuration. The stability of the system has been experimentally evaluated by [?] and compared with numerical results obtained by AVSP assuming no acoustic losses. These losses can be obtained experimentally [?] and are given for the two flames : $\alpha_A = 82(s^{-1})$ for flame A and $\alpha_B = 125(s^{-1})$ for flame B with an uncertainty of $\Delta\alpha = \pm 10(s^{-1})$. Numerically, stable regime is considered if the growth rate ω_i is smaller than the damping rate α, and unstable if the growth rate is larger than the damping rate. When considering the error $\Delta\alpha$, this classification becomes :

Cases studied		l3=100	l3=150	l3=200	l3=400
Expe./Simu.	l1=96.0	**C01**	**C02**	**C03**	**C04**
Expe./Simu.	l1=160.0	**C05**	**C06**	**C07**	**C08**
Expe./Simu.	l1=224.0	**C09**	**C10**	**C11**	**C12**

TABLE 1. Twelve different configurations explored : l_1 indicates the upstream manifold length and l_3 corresponds to the combustion chamber length. Dimensions are given in millimeters. From ref. [?]

– - Stable $\mathbf{S}$: $\omega_i < \alpha - \Delta\alpha$
– - Unstable $\mathbf{U}$: $\omega_i > \alpha + \Delta\alpha$
– - Marginal $\mathbf{S/U}$: $\alpha - \Delta\alpha < \omega_i < \alpha + \Delta\alpha$

The comparison between the experiment and the numerical results provided by [?] reveals a good agreement as illustrated in (Table. 2).

Case	**Flame A**				**Flame B**			
	C01	*C02*	*C03*	*C04*	*C01*	*C02*	*C03*	*C04*
Experiment	**S**	**S**	**S**	**U**	**S**	**S**	**S-U**	**U**
Simulation	**S**	**S**	**S**	**U**	**S**	**S**	**S-U**	**U**
	C05	*C06*	*C07*	*C08*	*C05*	*C06*	*C07*	*C08*
Experiment	**S**	**S**	S-U	**U**	**S**	**S**	**S**	UU
Simulation	**S**	**S**	S-U	**U**	**S**	**S**	**S-U**	**U**
	C09	*C10*	*C11*	*C12*	*C09*	*C10*	*C11*	*C12*
Experiment	**S**	**S**	**S-U**	**U**	**S**	**S**	**S-U**	**U**
Simulation	**S**	**S**	**U**	**U**	**S**	**S**	**S**	**U**

TABLE 2. Linear stability analysis of flame A and flame B. Comparison between experimental and numerical results. (S) Stable, (S/U) Marginally stable/unstable, (U) Unstable. The geometrical configurations C01 to C12 are defined in Table. 1.

However, three partial disagreements are observed and correspond to cases where the experiment gives a marginal stability ($\mathbf{S-U}$) while the computation predicts an instability ($\mathbf{U}$) or vice versa. In the remaining of the paper, one focuses on the operating point which corresponds to the configuration 07 for the Flame B where partial disagreement has been found between the experiment and numerical simulation.
Moreover, it is hardly conceivable to perform a computation for all the configurations as one Helmholtz computation takes almost 10 minutes when using 24 processors.

4 Uncertainty quantification study

Computing the risk factor (Eq. 4) associated to the first acoustic mode ($f_0 = \frac{\omega_0}{2\pi} = 121Hz$), i.e. the probability for this mode to be unstable constitutes one objective of this paper. Using uncertainty quantification is justified since repeating some tasks in this experiment may yield different results.
They can be related to a statistical distribution of the FTF uncertain parameters n and τ. In the context of non-intrusive methods where the acoustic code acts as a "black box", the choice of sampling points is essential. The next section details the classical brute force Monte Carlo analysis to provide a reference database for the growth rate probability density function (PDF), a necessary quantity to compute the risk factor (Eq. (4)). Then, surrogate models are fitted using few Helmholtz simulations extracted from the Monte Carlo database by solving a least mean square

problem. These surrogate models are then reused to perform a Monte Carlo analysis at reduced cost and estimate the risk factor. Finally, a discussion on the prediction of the risk factor is carried out by evaluating the accuracy of the low-order models against the initial full Monte Carlo method.

4.1 Classical Monte-Carlo analysis

First, a Monte Carlo sampling is used on the two dimensional parameters space n and τ (Eq. 3) to evaluate the probability of the first acoustic mode ($f_0 = \frac{\omega_0}{2\pi} = 121Hz$) to be unstable. The literature does not confer a clear accurate analysis on the uncertainty range of these parameters and this may have an impact on the stability of the system. We thus analysed some unpublished data from experimentalists at EM2C (Paris) and IMFT (Toulouse), two leading groups regarding the experimental measurement of flame response. Typically, data corresponding to the same configuration but gathered at different days were analysed to obtain an assessment of the variability of n and τ : from this variation, standard deviation of the FTF parameters σ_n and σ_τ are fixed to $\frac{\sigma_n}{\bar{n}} = \frac{\sigma_\tau}{\bar{\tau}} = 10\%$, where $\bar{n} = 1080J/m$ and $\bar{\tau} = 4.73ms$ correspond to the nominal experimental values. From these very scarce data, we decided to keep 10 % uncertainty for both input. In absence of more information regarding the probability density functions, two different distributions have been considered : a Uniform distribution (Section 4.2) and a β-distribution (Section 4.3) with the same mean and variance. The ranges of the uniform distributions are directly deduced from the experimental values of the amplitude and time delay i.e 10% of the mean values (Fig. (3)).

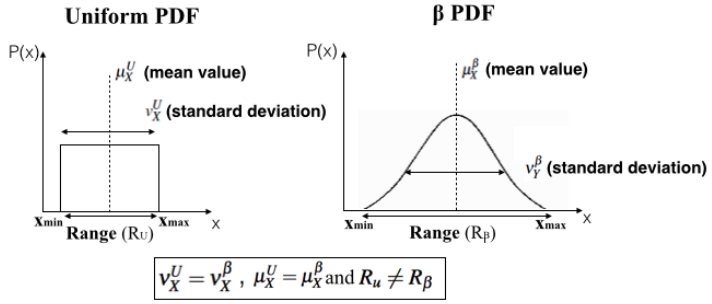

FIGURE 3. The uniform and the β-PDF of an arbitrary random variable X with similar mean (μ) and standard deviation (σ), but with different range (R)

The uniform PDF reads :

$$f_X^U = \mathbb{1}_{[x_{max}-x_{min}]} \frac{1}{||x_{max}-x_{min}||} \quad \text{for} \quad x_{min} \leq x \leq x_{max} \tag{5}$$

Therefore, the mean μ_X^U and the variance v_X^U are :

$$\mu_X^U = \frac{x_{min}+x_{max}}{2} \quad \text{and} \quad v_X^U = \frac{1}{12}(R_U \mu_X^U)^2 \tag{6}$$

where R_U represents the normalized range $\frac{x_{max}-x_{min}}{\mu_X^U}$ of the uniform distribution : here $R_U = 10\%$.
The β-distribution is characterized by its density function :

$$f_Y^\beta = B(\alpha,\beta)^{-1} y^{\alpha-1}(1-y)^{\beta-1} \quad \text{for} \quad 0 \leq y \leq 1 \tag{7}$$

where $B(\alpha,\beta)$=$\frac{\Gamma(\alpha)\Gamma(\beta)}{\Gamma(\alpha+\beta)}$ denotes the beta function, $\Gamma(.)$ is the gamma function, and α and β are two free parameters. Note that f_Y^β is only defined for a reduced random variable Y on [0, 1]. The parameters α and β which characterize the β-PDF are deduced from the desired mean μ_Y^β and variance v_Y^β of this reduced variable Y :

$$\alpha = \mu_Y^\beta \left(\frac{\mu_Y^\beta(1-\mu_Y^\beta)}{v_Y^\beta} - 1 \right) \tag{8}$$

and

$$\beta = (1-\mu_Y^\beta) \left(\frac{\mu_Y^\beta(1-\mu_Y^\beta)}{v_Y^\beta} - 1 \right) \tag{9}$$

To close the problem, the reduced variable Y in [0, 1] is related to the desired random variable X in $[x_{min}, x_{max}]$:

$$X = \mu_X^\beta(1 + R_\beta[2Y-1]) \tag{10}$$

Taking the mean and variance of the previous equation leads to the following relations between characteristics of X and Y :

$$\mu_Y^\beta = 1/2 \text{ and } v_Y^\beta = \frac{v_X^\beta}{4R_\beta^2}(\mu_X^\beta)^2 \tag{11}$$

Consequently, the mean value of Y is fixed and its variance can be deduced by imposing that the beta and Uniform PDFs have

the same characteristics, i.e. $\mu_X^\beta = \mu_X^U$ and $\nu_X^\beta = \nu_X^U$. Note however, that the range of the β-PDF appears in (μ_X^β)(Eq. (11)). If this range is chosen equal to the range of the previous uniform PDF (i.e. $R_\beta = R_U = 10\%$) then the β-distribution degenerates to the previous uniform PDF. Consequently, the range R_β is an additional free parameter. For this study, this range is fixed to $R_\beta = 30\%$ leading to the characteristic values $\alpha = \beta = 2.87$. In the following sections, the results from these two distributions are described and the statistical convergence of the risk factor is discussed.

4.2 The uniform distribution

The Monte Carlo sampling is displayed in Fig. 4 for the configuration 07 of the Flame B. Each point of Fig. 4 corresponds to a Helmholtz simulation in the complex domain. The horizontal solid lines denotes the acoustic losses $\alpha : 115\ s^{-1} < \alpha_B < 135\ s^{-1}$. The stable or unstable regions are evaluated using the difference $\omega_i - \alpha$:

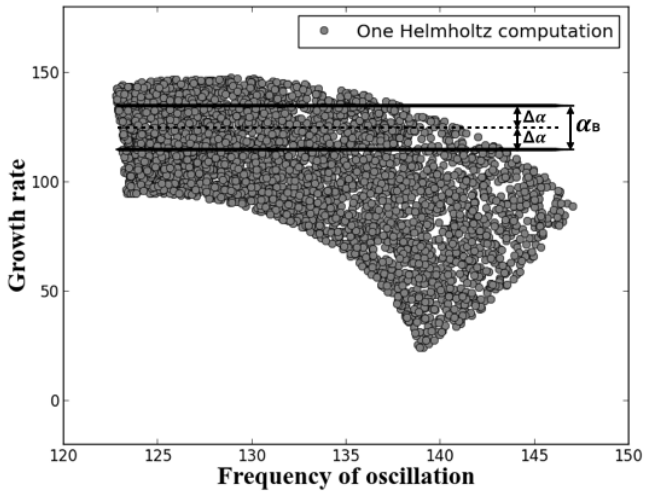

FIGURE 4. Monte Carlo results for the configuration 07 for the Flame B. Uncertain region for the first acoustic mode.

1. $\omega_i - 115\ s^{-1} < 0$ corresponds to a stable system (**S**).
2. $\omega_i - 135\ s^{-1} > 0$ corresponds to a unstable system (**U**).
3. $115\ s^{-1} < \omega_i < 135\ s^{-1}$ corresponds to a situation where the system is marginal (neither stable nor unstable) (**S/U**).

The 4000 samples are then classified into three types : stable regime (**S**), unstable regime (**U**) and marginal regime (**S/U**). The histogram of the growth rate is shown in Fig. 5 and corresponds to an approximation of the growth rate Probability Density Function PDF(ω_i). Most of the thermoacoustic modes found by AVSP are in the stable regime. This leads to a risk factor close to 24 %.

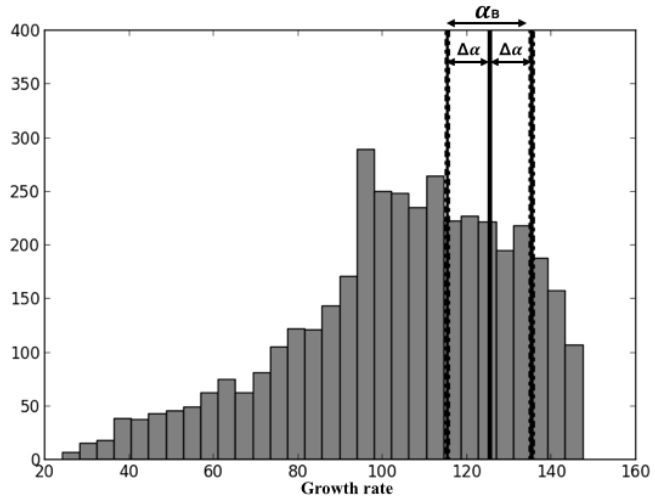

FIGURE 5. Histogram of the growth rate of acoustic disturbance for 4000 samples using the Uniform distribution for the parameters n and τ.

4.3 The β-distribution

Following a similar methodology, 4000 runs are performed using the AVSP code when n and τ follow a β-distribution. A

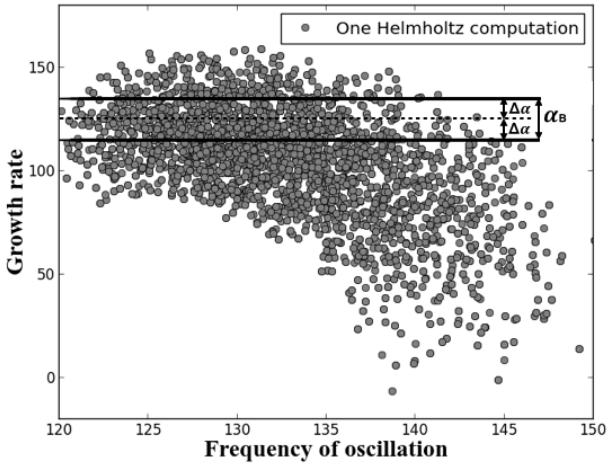

FIGURE 6. Monte Carlo results for the configuration 07 for the Flame B. Uncertain region for the first acoustic mode.

stability analysis is performed to classify each Helmholtz solution as stable (**S**), unstable (**U**) and marginal (**S/U**) (Fig. 6). As expected, the scatter plot is more diffused than in the case of the Uniform PDF because extrema values are less expected than intermediate ones when using the β distribution. The histogram of the growth rate is plotted in Fig. 7 where the medium value of the acoustic loss is reported ($\bar{\alpha}_B = 125\ s^{-1}$, solid vertical line). From this histogram, a risk factor close to 22 % is obtained. The

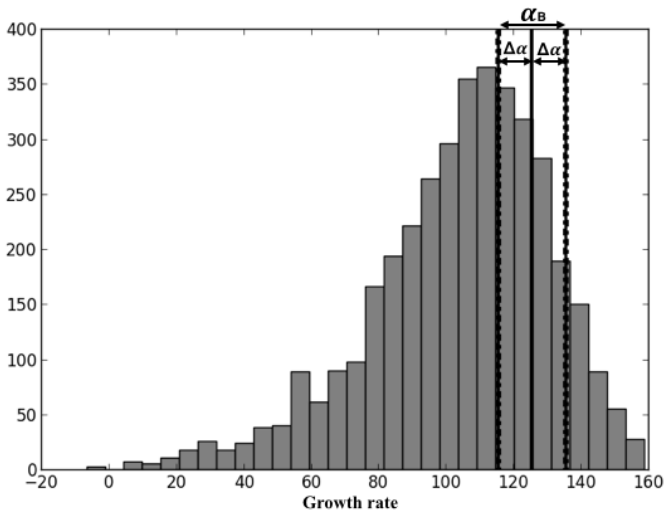

FIGURE 7. Histogram followed by the growth rate of acoustic disturbance for 4000 samples using the Uniform distribution for the parameters n and τ.

risk factor obtained from the Uniform and Beta distribution are close (24 % vs 22%) showing that UQ results are weakly affected by the distributions chosen for the input parameters n and τ for this case. This suggests that assessing the risk factor of a mode without a clear knowledge of the uncertainties on the input data is relevant.

4.4 Convergence study

For both the uniform and β-distribution, a brute force Monte Carlo analysis is performed using 4000 runs. Nevertheless, the question of the convergence of the resulting risk factor is still open. Consequently, a convergence study is realized by doing the same exercise but with other dataset size : from 100 to 4000. The results of this study are displayed in Fig. 8.
In both figures, the dashed line represents the risk factor of the system determined by the full Monte Carlo database with 4000 runs and the solid line corresponds to the variation of the risk factor. This study reveals that 4000 samples are by far sufficient to reach a reliable convergence of the risk factor.

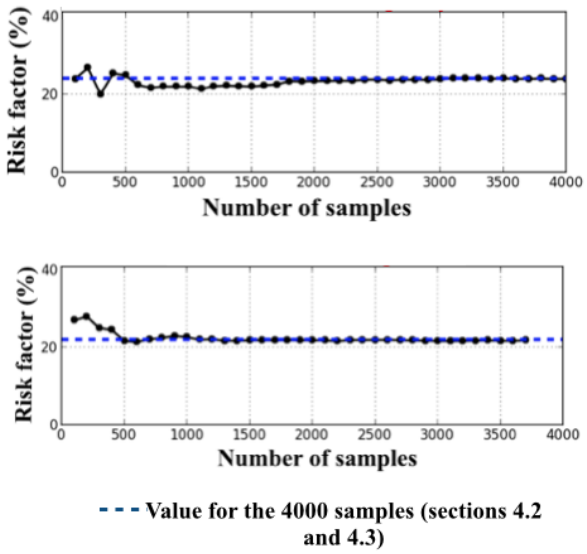

FIGURE 8. Convergence study of the risk factor (in %) ; Top : Uniform distribution, Bottom : β-distribution

This method is relatively simple to implement and affordable when few parameters (in our case n and τ) are involved but becomes expensive when the dimensionality increases (this is typically the case for annular combustors fed by several burners) or when the CPU cost for each computation is large. This suggests that reduced methodologies have to be introduced to obtain risk factors in more complex configurations : this is the second objective of this paper discussed in the following.

5 Multiple linear regression

Because Eq. (2) is an eigenvalue problem which is nonlinear in the pulsation ω_i, the surface response $\omega_i = \omega_i(n,\tau)$ is implicit and non-linear. To speed up the UQ analysis, it is worth investigating if this surface response can be approximated by explicit surrogate models. Two such models are tested in this paper :

1. One based on the n-τ parameters :

$$Y^{model_1} = \beta_0 + \beta_1 n + \beta_2 \tau \tag{12}$$

2. One based on the Flame Transfer Function evaluated at $\omega = \omega_0$ where ω_0 corresponds to the mode without flame coupling. FTFs incorporate here physical non-linearities into the model :

$$Y^{model_2} = \beta_0 + \beta_1 \Re(ne^{j\omega_0\tau}) + \beta_2 \Im(ne^{j\omega_0\tau}) \tag{13}$$

These two algebraic models can be written in linear algebra notation as follows :

$$Y = X\beta + \varepsilon = Y^{model} + \varepsilon \tag{14}$$

where $X\beta$ is the matrix-vector product, $\beta = [\beta_0, \beta_1, \beta_2]^T$ corresponds to the regression coefficients of the model. These coefficients represent the mean change in the response variable for one unit of change in the predictor variable. Y is a N $\times$ 1 dimensional vector containing the growth rate ω_i determined from N Helmholtz computations, X is the matrix containing 1, n and τ for each samples and ε the N$\times$1 vector of residuals :

$$Y = \begin{bmatrix} Y_1 \\ Y_2 \\ \vdots \\ Y_N \end{bmatrix}, X = \begin{bmatrix} 1 & n_1 & \tau_1 \\ 1 & n_2 & \tau_2 \\ \vdots & \ddots & \vdots \\ 1 & n_N & \tau_N \end{bmatrix}, \beta = \begin{bmatrix} \beta_0 \\ \beta_1 \\ \beta_2 \end{bmatrix} \text{ and } \varepsilon = \begin{bmatrix} \varepsilon_1 \\ \varepsilon_2 \\ \vdots \\ \varepsilon_N \end{bmatrix}$$

Since models of Eq. (12) are linear, a least squares methodology is used to determine the coefficients β which minimize the error ε :

$$\tilde{\beta} = \left(X^t X\right)^{-1} X^t Y \tag{15}$$

where $\tilde{\beta}$ corresponds to the estimated parameters from the least squares, $(X^t X)^{-1}$ is called the "information matrix" and X^t corresponds to the transpose of the X matrix. The predicted values $\tilde{Y}$ for the mean of Y are then determined as follows :

$$\tilde{Y} = X\tilde{\beta} = X\left(X^t X\right)^{-1} X^t Y \tag{16}$$

A Monte Carlo analysis is performed at reduced cost to provide an approximate risk factor for the mode of interest $f_0 = \frac{\omega_0}{2\pi} = 121Hz$. A two-steps UQ strategy is investigated in the following :

1. Find the three regression coefficients associated to the models at reasonable cost using Eq (15) and only few Helmholtz computations .
2. Use the two surrogate models to perform a Monte Carlo analysis for assessing the risk factor.

The correlation coefficient is evaluated to measure the correlation between the two surrogate models (Eq (12) and Eq (13)) and the reference Monte Carlo database obtained in section 4 :

$$Corr^2 = \sqrt{\frac{\sum_i (Y^{model} - \bar{Y})^2}{\sum_i (Y - \bar{Y})^2}} \tag{17}$$

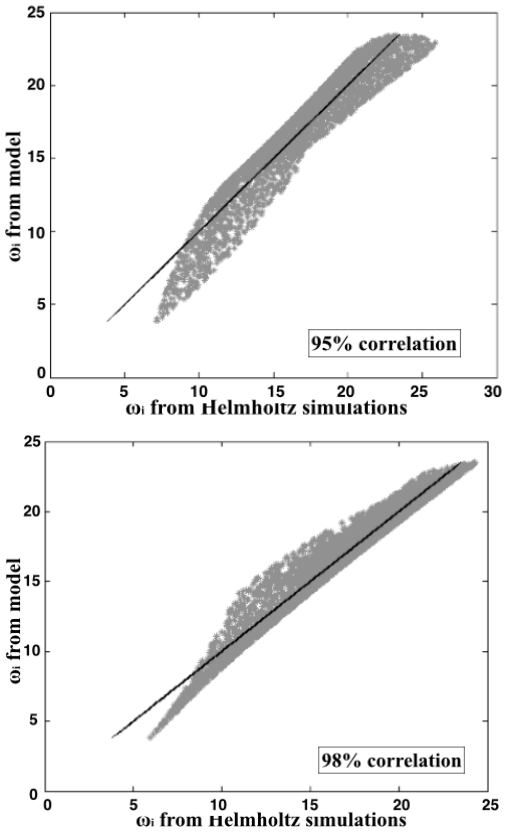

FIGURE 9. Multiple linear regression computation ; Top : Using the linear model 1 Eq (12), Bottom : Using linear model 2 Eq (13).

The correlation is 95% for the linear model 1 (Eq (12)) and 98% correlation for the linear model 2 (Eq (13)). The corresponding growth rates are plotted against their exact counterpart in Fig. 9. The algebraic surrogate model using the FTF formulation (Eq (13)) is rather accurate in mimicking the actual surface response of the system. That is the reason why the latter is then used to plot the histogram of the growth rate based on the reference Monte Carlo database using 4000 runs for both the Uniform and the Beta distribution, see Fig. 10.

The shape of both histograms is very similar to the histograms plotted previously in section 4 for the Uniform and β distributions. Also, the associated risk factor is approximated using the surrogate model 2 : (i) for the Uniform distribution the RF is close to 23% (ii)for the β-distribution the RF is close to 21% . The next step is to use Eq (13) with the aim to find a way to approximate the risk factor at low cost i.e. relying on much less then 4000 Helmholtz computations. To assess the number of Helmholtz computations required to tune the surrogate model, several tuning of the β coefficients are performed based on 3, 5, 10, 40, 70 and 100 Helmholtz computations (instead of 4000

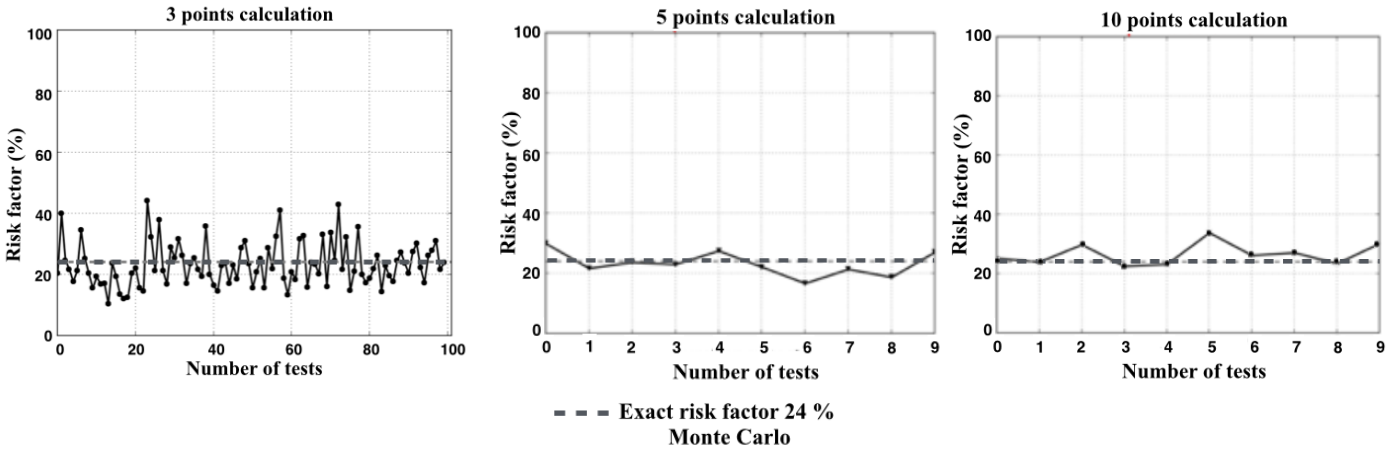

FIGURE 11. Risk factor from Eq (13) ; Left : 3 points calculations are used, Middle : 5 points calculations are used, Right :10 points calculations are used

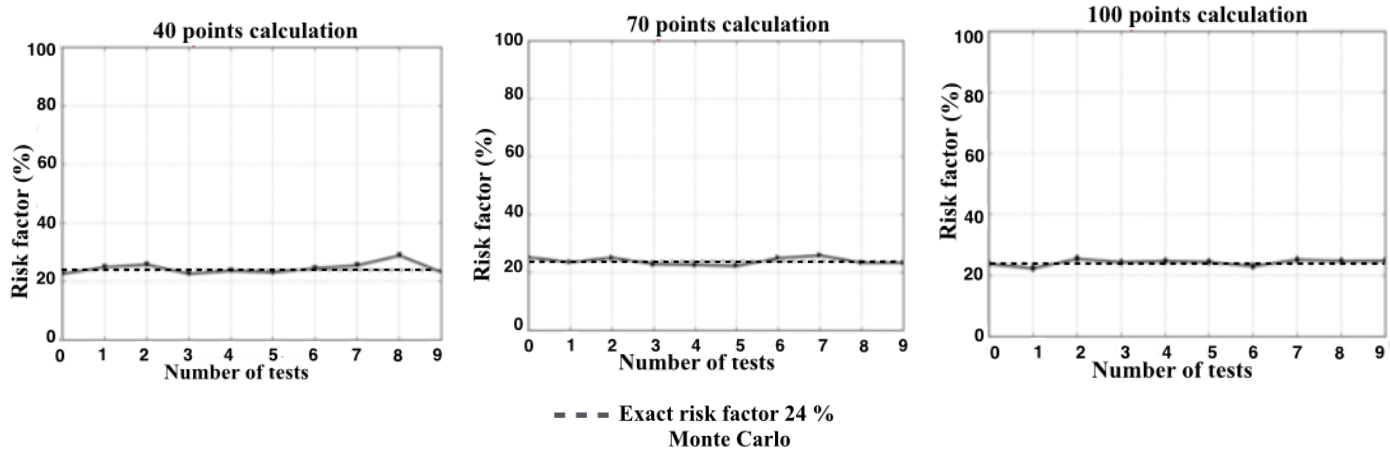

FIGURE 12. Risk factor from Eq (13) ; Left : 40 points calculations are used, Middle : 70 points calculations are used, Right :100 points calculations are used

Helmholtz simulations). This analysis is performed one hundred times using 3 Helmholtz computations to evaluate the variation of the risk factor. Then, this analysis is done ten times, changing arbitrary the 5, 10, 40, 70 and 100 Helmholtz computations chosen out of 4000 samples database. The corresponding risk factors are displayed in Fig. 11 and Fig. 12. The gray dashed lines in all figures represent the reference risk factor equal to 24% obtained by the Monte Carlo analysis over 4000 Helmholtz computations. A good agreement is observed showing that only 100 simulations give an accurate risk factor. Even 3 points tuning of the β-coefficients leads to a "reasonnable" approximation of the risk factor, between 10 and 43%. The results reveal that a purely algebraic model is able to fairly assess at reduced cost the risk factor of thermoacoustic modes. Using approximately ten Helmholtz simulations is sufficient to accurately estimate the risk factor of the system.

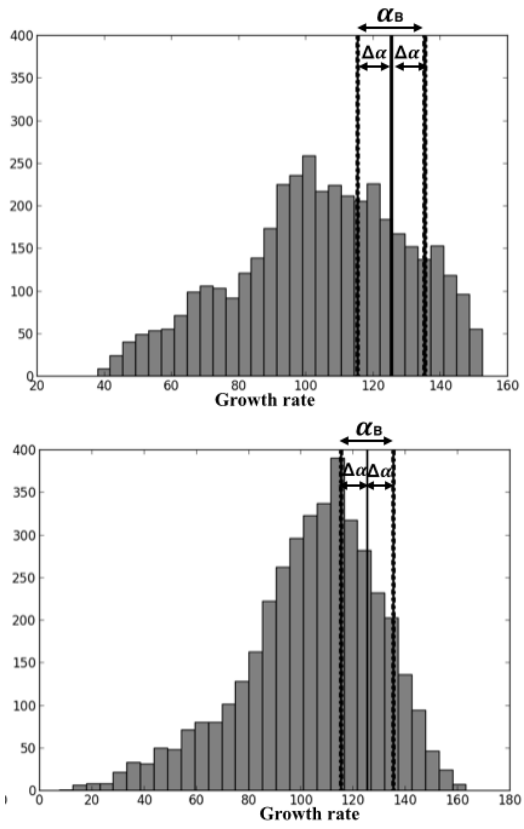

FIGURE 10. Histogram followed by the growth rate using algebraic surrogate model 2(Eq (13)) : Top : With the full Monte Carlo database using the Uniform Distribution, Bottom : With the full Monte Carlo database using the β-distribution

CONCLUSIONS

In this paper, a UQ study applied to thermoacoustic instabilities in a single swirled combustor experiment has been carried out. An Helmholtz solver has been used to analyze the thermoacoustic modes of the combustion chamber. The FTF measured experimentally is used as a flame model for the Helmholtz solver. The frequency of oscillation as well as the growth rate of the first thermoacoustic mode are computed in 24 different operating points. The stability of the system has been evaluated by [?] and predictions show a good agreement with experimental behavior of the combustor. However, it also reveals that uncertainties on the Flame Transfer Function parameters may lead to modes which are marginally stable/unstable. Towards a more accurate mode classification instead of the usual stable/unstable one, a continuous description has been adopted based on the risk factor defined as the probability for a mode to be unstable given the uncertainties on the input parameters. The risk factor associated to the first acoustic mode of the combustor has been evaluated using a Monte Carlo analysis based on 4000 Helmholtz simulations of a single experimental operating point but with random perturbations on the FTF parameters. The analysis of the Monte Carlo database suggests that a two-step UQ strategy may be efficient to deal with thermoacoustics in such a system. First, two bilinear surrogate models were tuned from a moderate number of Helmholtz solutions (a few tens). Then, these algebraic models were used to perform a Monte Carlo analysis at reduced cost and approximate the risk factor of the mode. A comparison between the reference risk factor given by the full Monte Carlo database and the approximate risk factor obtained by the surrogate models shows a good agreement which proves that reduced efficient methods can be used to predict unstable modes.

ACKNOWLEDGEMENTS

This study was performed within the UMRIDA project funded by the European commission (FP7-AAT-2013-RTD-1 - 605036). The authors also thank the Center for Turbulence Research for its support during the 2014 Summer Program. Prof. G. Iaccarino (Stanford University) and P. Constantine (Umines Colorado) are acknowledged for their help regarding the UQ strategy.

Rfrences

[1] CROCCO, L. Aspects of combustion instability in liquid propellant rocket motors. part II. *22* (1952), 7–16.

[2] DOWLING, A. P. The calculation of thermoacoustic oscillations. *180*, 4 (1995), 557–581.

[3] NICOUD, F., BENOIT, L., SENSIAU, C., AND POINSOT, T. Acoustic modes in combustors with complex impedances and multidimensional active flames. *45* (2007), 426–441.

[4] PALIES, P. *Dynamique et instabilités de combustion de flammes swirlées*. Phd thesis, Ecole Centrale Paris, 2010.

[5] PALIES, P., DUROX, D., SCHULLER, T., AND CANDEL, S. The combined dynamics of swirler and turbulent premixed swirling flames. *157* (2010), 1698–1717.

[6] PALIES, P., DUROX, D., SCHULLER, T., AND CANDEL, S. Nonlinear combustion instability analysis based on the flame describing function applied to turbulent premixed swirling flames. *158*, 10 (2011), 1980 – 1991.

[7] POINSOT, T., AND VEYNANTE, D. *Theoretical and Numerical Combustion*. Third Edition (www.cerfacs.fr/elearning), 2011.

[8] SCHULLER, T., DUROX, D., PALIES, P., AND CANDEL, S. Acoustic decoupling of longitudinal modes in generic combustion systems. *Combustion and Flame 159* (2012), 1921–1931.

[9] SILVA, C. F., NICOUD, F., SCHULLER, T., DUROX, D., AND CANDEL, S. Combining a Helmholtz solver with the

flame describing function to assess combustion instability in a premixed swirled combustor. *160*, 9 (2013), 1743 – 1754.

[10] WILLIAMS, F. A. *Combustion Theory*. Benjamin Cummings, Menlo Park, CA, 1985.